Grain-size-sensitive seismic wave attenuation in polycrystalline olivine

Ian Jackson, John D. Fitz Gerald, Ulrich H. Faul, and Ben H. Tan
Research School of Earth Sciences, Australian National University, Canberra ACT, Australia

Received 17 September 2001; revised 6 February 2002; accepted 11 February 2002; published 21 December 2002.

[1] In order to investigate the processes responsible for the attenuation of seismic shear waves in the Earth's upper mantle, four olivine polycrystals ranging in mean grain size d from 3 to 23 μm have been fabricated, characterized, and mechanically tested in torsion at high temperatures and seismic frequencies. Both the shear modulus, which governs the shear wave speed V_S, and the dissipation of shear strain energy Q^{-1} have been measured as functions of oscillation period T_o, temperature T, and, for the first time, grain size. At sufficiently high T all four specimens display similar absorption band viscoelastic behavior, adequately represented for $1000 < T < 1200$ or 1300°C and $1 < T_o < 100$ s, by the expression $Q^{-1} = A\,[T_o d^{-1} \exp(-E/RT)]^{\alpha}$ with $A = 7.5 \times 10^2$ s$^{-\alpha}$ μm$^{\alpha}$, $\alpha = 0.26$ and $E =$ 424 kJ mol^{-1}. This mildly grain-size-sensitive viscoelastic behavior of melt-free polycrystalline olivine is attributed to a combination of elastically and diffusionally accommodated grain boundary sliding, the latter becoming progressively more important with increasing T and/or T_o. Extrapolation to the larger (mm-cm) grain sizes expected in the Earth's upper mantle yields levels of dissipation comparable with those observed seismologically, implying that the same grain-size-sensitive processes might be responsible for much of the observed seismic wave attenuation. The temperature sensitivity of V_S is increased substantially by the viscoelastic relaxation allowing the lateral variability of wave speeds to be associated with relatively small temperature perturbations. *INDEX TERMS:* 5144 Physical Properties of Rocks: Wave attenuation; 3909 Mineral Physics: Elasticity and anelasticity; 5120 Physical Properties of Rocks: Plasticity, diffusion, and creep; 3902 Mineral Physics: Creep and deformation; 3904 Mineral Physics: Defects; *KEYWORDS:* anelasticity, viscoelasticity, seismic wave attenuation, olivine, grain boundary sliding

Citation: Jackson, I., J. D. Fitz Gerald, U. H. Faul, and B. H. Tan, Grain-size-sensitive seismic wave attenuation in polycrystalline olivine, *J. Geophys. Res.*, *107*(B12), 2360, doi:10.1029/2001JB001225, 2002.

1. Introduction

[2] The Earth's upper mantle beneath the lithosphere is distinctive seismologically, being a zone of generally low and laterally variable seismic wave speeds [e.g., *Grand and Helmberger*, 1984; *Su et al.*, 1994; *van der Hilst et al.*, 1998] and marked attenuation. The dissipation is predominantly in shear and is most pronounced at depths of about 80–220 km in the upper mantle where Q^{-1} exceeds 0.01 [*Romanowicz and Durek*, 2000]. Both the radial models and the superimposed lateral variability revealed by tomographic studies exhibit a strong spatial correlation between high attenuation and relatively low shear wave speeds. This association is suggestive of thermally activated viscoelastic behavior in the solid state [*Goetze*, 1977] and probably, at least locally, partial melting (e.g., beneath mid-ocean ridges [*Toomey et al.*, 1998]).

[3] Interpretation of these seismological observations requires an understanding of the viscoelastic behavior of ultramafic materials at high temperature and seismic frequency, established through experiments conducted under carefully controlled laboratory conditions. Note: Following *Nowick and Berry* [1972], we use the term "viscoelastic" to describe behavior that is linear, but neither instantaneous nor fully recoverable. Linearity is defined by *Nowick and Berry* [1972, p. 4] as follows: "If a given stress history $\sigma_1(t)$ produces the strain $\varepsilon_1(t)$ and if a stress $\sigma_2(t)$ gives rise to $\varepsilon_2(t)$ then the stress $\sigma_1(t) + \sigma_2(t)$ will give rise to the strain $\varepsilon_1(t) + \varepsilon_2(t)$." Equivalently, it is required that the governing differential equation involves stress, strain, and their respective time derivatives in linear combination.

[4] Studies of natural olivine-rich rocks with torsional forced oscillation/microcreep methods have revealed a pronounced strain energy absorption band ($Q^{-1} \sim \omega^{-\alpha}$ with $0.1 < \alpha < 0.3$) and associated frequency dependence (dispersion) of the shear modulus G at high subsolidus temperatures [*Berckhemer et al.*, 1982; *Jackson et al.*, 1992]. However, detailed interpretation of the observed behavior was significantly complicated by the occurrence of thermal microcracking, by the progressive dehydration of hydrous layer-silicate minerals, and, in the study of Berckhemer et al., by melting. More recently, the difficulties arising from the chemical complexity of natural rocks and the inevitable microcracking during thermal cycling of relatively coarse-grained materials have been circumvented

0148-0227/02/2001JB001225$09.00

Table 1. Polycrystalline Olivine (Fo_{90}) Specimens Employed in This Study

	Precursor Powder		Hot-Pressed (HP) and Mechanically Tested (AT) Specimens			
Specimen	Grain Size, μm	Heat Treatment	Jacket Material	Porosity,[a] % (HP)	Grain Size,[b] μm (AT)	$[H_2O]$,[c] wt ppm (AT)
6381	<1 (sol-gel)	oven-dried	Ni70Fe30	0.0	2.9	<10
6380	2–10 (SC)[d]	prefired	Ni70Fe30	0.0	6.5	<10
6365	<1 (sol-gel)	oven-dried	Ni70Fe30	0.3	12.4	75
6261	10–38 (SC)[e]	oven-dried	Fe	1.0	23.4	130

[a]Based on density of 3.338 g cm^{-3} for natural Fo_{90} olivine for specimens hot-pressed for 25 hours at 1200°C and 300 MPa, except for specimen 6261 (6 hours at 1300°C and 300 MPa).
[b]Mean grain size estimated as explained in the text.
[c]Mainly molecular water; A(3400 cm^{-1}) converted into $[H_2O]$ with free-water absorption coefficient of 81 cm^{-1} (mol $L^{-1})^{-1}$.
[d]San Carlos batch 2 (this study).
[e]San Carlos batch 1 [*Tan et al.*, 2001].

through promising exploratory studies of fine-grained synthetic materials [*Tan et al.*, 1997; *Gribb and Cooper*, 1998; *Tan et al.*, 2001]. Viscosities inferred from the torsional microcreep tests of these studies are similar to those associated with grain-size-sensitive behavior at the much larger strains of conventional deformation experiments. A diffusional origin and associated grain-size (d) sensitivity have therefore reasonably been invoked for the viscoelastic behavior responsible for the modulus dispersion and dissipation observed at seismic frequencies in these fine-grained aggregates.

[5] *Gribb and Cooper* [1998] argued that their observations on reconstituted dunite of 2.8 μm grain size at temperatures of 1200–1285°C reflect the transition from elastically accommodated grain boundary sliding (recoverable and hence anelastic) to diffusionally accommodated grain boundary sliding (irrecoverable and therefore viscous). Analysis in terms of the model of *Raj* [1975] allowed an extrapolation (in which $Q^{-1} \sim d^{-1}$ is implicit) to the range of grain sizes (1–10 mm) considered representative of the upper mantle, resulting in the speculation that such diffusional processes could contribute significantly to seismic wave attenuation only if subgrain size rather than grain size were the controlling variable. Subsequently, the behavior of a suite of more coarse-grained polycrystalline Fo_{90} olivine specimens ($8 < d < 150$ μm) has been intensively sampled across the entire elastic-anelastic-viscous transition, with qualitative indications of a substantially milder grain-size sensitivity [*Tan et al.*, 2001] with potentially different seismological implications.

[6] In this study we report the first robust measurements of the grain-size sensitivity of strain energy dissipation in fine-grained polycrystalline olivine. This new information allows a more secure extrapolation to the regime of seismic wave propagation in the Earth's upper mantle, providing a firm indication of the level of seismic wave attenuation contributed by grain-size-sensitive diffusional processes under subsolidus conditions.

2. Specimen Fabrication and Testing

[7] For this study three new fine-grained Fo_{90} olivine polycrystals have been prepared by hot isostatic-pressing from either natural or synthetic precursor materials. The procedures for preparation of high-purity grain-size-sorted powders from olivine phenocrysts from San Carlos (Arizona) have previously been described [*Tan et al.*, 2001]. The synthetic precursor material was prepared by dissolving Mg and Fe nitrates in ethanol and adding tetraethyl orthosilicate to this solution. Gelation was induced by addition of a few drops of nitric acid and slow heating above room temperature. The gel was dried at successively higher temperatures up to 1050°C, ground, pelletized and crystallized under appropriately controlled oxygen atmosphere at 1400°C. In order to minimize any residual inhomogeneity the pellets were reground and run again under the same conditions. The olivine in the resulting porous aggregates had a maximum grain size <1 μm. The aggregates were reground and, like the natural precursor material, cold-pressed into pellets that were either oven-dried or prefired at 1200°C under controlled atmosphere prior to encapsulation either in Fe or $Ni_{70}Fe_{30}$ containers for hot isostatic-pressing within an internally heated gas-charged pressure vessel.

[8] Cylindrical samples (of 30 mm length and ~12 mm diameter) were precision ground from the hot-pressed specimens and wrapped in Fe (specimen 6261 [*Tan et al.*, 2001]) or $Ni_{70}Fe_{30}$ foil for mechanical testing with torsional forced oscillation/microcreep methods [*Jackson and Paterson*, 1993; *Jackson et al.*, 2000]. Each specimen was first annealed for an extended period (~20–60 hours) at the hot-pressing temperature (and 200 MPa confining pressure). During this interval, forced oscillation and microcreep tests were repeatedly conducted in order to monitor any time dependence in the mechanical behavior that might reflect microstructural evolution. Significant temporal evolution toward higher modulus and lower dissipation was observed during the first 10 hours of reexposure of specimens 6381, 6365, and 6261 to the hot-pressing temperature, but no systematic changes were seen for specimen 6380. The temperature dependent mechanical response of each specimen is best constrained by the results obtained toward the end of the annealing period along with those obtained during subsequent slow staged cooling (1–2°C min^{-1}) under pressure to room temperature.

3. Specimen Characterization

[9] Examination of the specimens before and after mechanical testing reveals little grain growth during mechanical testing. The mean grain sizes determined on the specimens following mechanical testing (Table 1), ranging from 3 to 12 μm, are regarded as closely representative of the material under test. SEM and TEM observa-

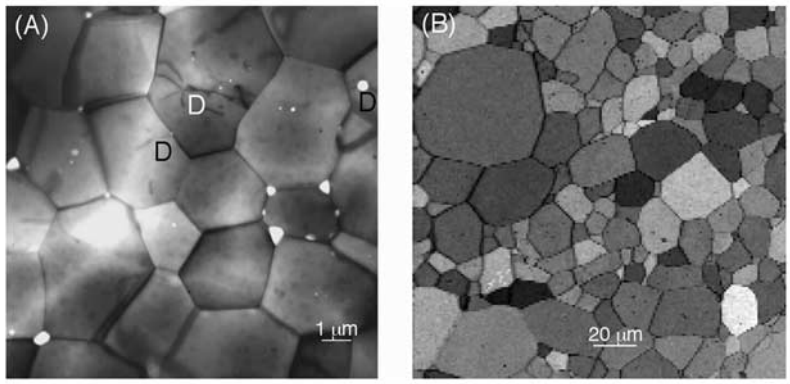

Figure 1. Microstructures of the most fine-grained (Figure 1a) and the most coarse-grained (Figure 1b) samples in this study. (a) TEM bright field image of sample AT6381. The sol-gel derived samples have a uniform grain-size distribution with near ideal "foam textures" and gently curved grain boundaries. Pores are white in this image. The dark lines above the letter D are dislocations; most grains however are free of dislocations and none shows subgrain boundaries. (b) Band contrast image from an electron-backscatter diffraction (EBSD) map of sample AT6261. Band contrast is a measure of pattern quality; orientation dependent pattern quality and the poor contrast due to overlapping patterns at grain boundaries make it easy to identify grains. The grain-size distributions of the samples derived from San Carlos olivine extend to larger normalized grain size than their sol-gel counterparts (Figure 2), but the grain shapes are similarly equant with smoothly curved grain boundaries. None of the samples has lattice preferred orientation.

tions on the specimens after testing show that they are texturally well-equilibrated with generally low dislocation densities and very few subgrain boundaries, particularly in the sol-gel derived materials (Figure 1). The chemical analyses presented in Table 2 indicate very low levels of impurity in the olivine polycrystals derived from both the natural and synthetic precursors. In the sol-gel derived samples Ca is the only trace element detectable by WDS analysis. Trace amounts of quenched silicate melt glass ($\ll$ 0.1%) located primarily in grain edge triple junctions are found by TEM in the specimens derived from San Carlos olivine but no melt has been detected in the specimens of sol-gel origin. Specimens of sol-gel origin contain 1–2 vol % of widely dispersed clusters of orthopyroxene grains.

[10] Grain sizes were obtained from scanning electron microscope (SEM) electron backscatter diffraction (EBSD) mapping, and for specimen AT6381 also from transmission electron microscope (TEM) micrographs. Grain-size distributions approach those expected for normal grain growth, but, particularly for the samples derived from San Carlos olivine, with a "tail" reflecting the presence of a few large grains which are volumetrically significant (Figure 2). In order to limit grain growth, the samples of this study were exposed to a maximum temperature of 1200°C during hot pressing and subsequent mechanical testing.

[11] Mean grain sizes (Table 1) were determined as follows. The diameter is calculated for the circle equivalent in area to each grain represented in an image of a 2-D section. The unweighted average "equivalent circle" diameter, multiplied by $4/\pi$ (=1.27) to allow for sectioning bias, provides an estimate of average grain size comparable with that derived by conventional linear intercept methods (e.g., d = 30 μm for specimen 6261 [*Tan et al.*, 2001]).

4. Data Analysis

[12] The raw data from both forced-oscillation and microcreep tests were processed to yield results in the form of shear modulus G and dissipation Q^{-1} versus period T_o typically for the interval 1–100 s [*Jackson*, 2000]. Additional information concerning the response at longer periods (to 1000 s) was obtained at selected temperatures from forced-oscillation and microcreep tests of longer duration. The viscoelastic behavior of the combination of mild steel jacket and Fe or $Ni_{70}Fe_{30}$ liner was modeled with data

Table 2. Composition of Sol-Gel and San Carlos Olivine-Derived Specimen (WDS Analysis)[a]

	SiO_2, wt %	FeO, wt %	MnO, wt %	NiO, wt %	MgO, wt %	CaO, wt ppm	Cr_2O_3, wt ppm	Mg #
AT6381 (Sol-gel)								
Scan	40.76(36)	10.08(38)	nd	nd	49.15(38)	nd	nd	
Spot	40.73(6)	10.18(33)	nd	nd	49.08(28)	100(10)	nd	89.6
AT6261 (San Carlos)								
Scan	40.20(33)	8.98(33)	0.12(1)	0.32(3)	50.29(24)	880(70)	220(100)	
Spot	40.25(22)	9.14(17)	0.13(1)	0.27(4)	50.12(16)	920(20)	190(60)	90.7

[a]Each scan analysis was obtained from a 12 by 12 μm area including grain boundaries, spot analyses from grain interiors. nd, not detected.

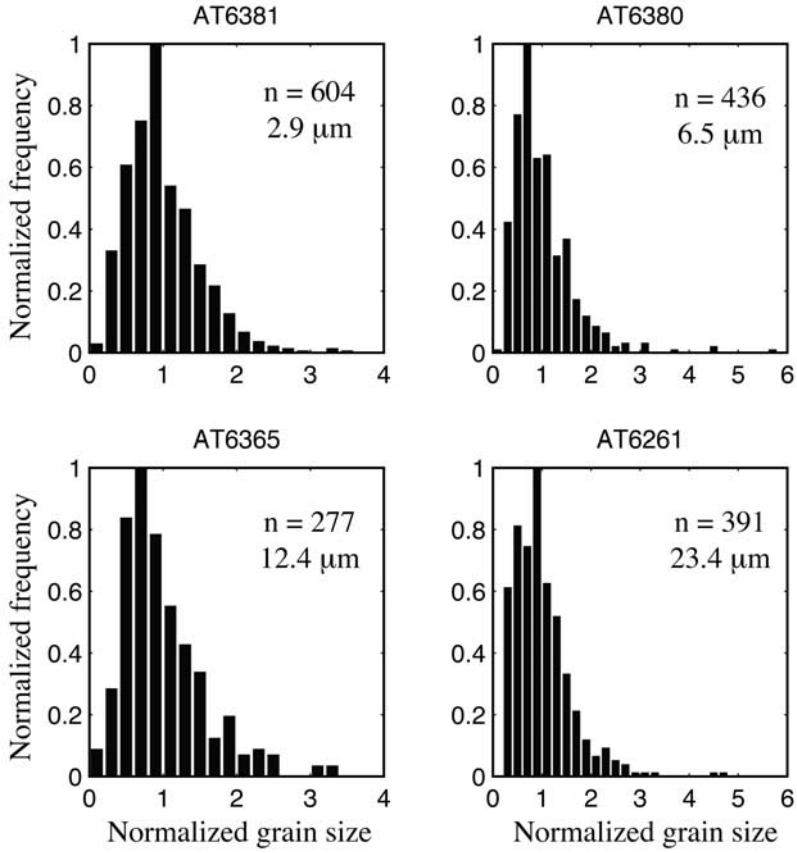

Figure 2. Normalized grain-size distributions of the four specimens used in this study. (left) Two sol-gel derived specimens and (right) two San Carlos olivine-derived specimens. Grain sizes were determined from EBSD maps of parts of a section of each sample. The maps were acquired on a SEM with W-filament and software from HKL. The mean grain size and the number of grains are shown in the histograms. Grain-size measurements of the most fine-grained sample, AT6381, were made both on TEM photomicrographs and an EBSD map resulting in nearly identical mean grain sizes (2.8 and 2.9 μm, respectively). The San Carlos samples have a broader grain-size distribution, particularly AT6380 with a few very large grains.

obtained from similar forced oscillation measurements on mild steel for $1 < T_o < 100$ s [*Jackson et al.*, 2000] extrapolated as required to longer periods through equation (5) below. This approximation is least satisfactory when the shear modulus of the specimen is lowest (for the longest periods, highest temperatures and smallest grain sizes) because the relative contribution of the jacket plus liner to the overall torsional stiffness is greatest under these conditions. The implications are therefore potentially more severe for the inferred values of viscosity than for dissipation and modulus dispersion within the 1–100 s band.

[13] For temperatures $\leq$900°C the behavior of each of the tested specimens is essentially elastic, with minimal dissipation and with shear moduli closely consistent with the $G(T)$ trend expected for a dense polycrystal from high-frequency (MHz) single-crystal data [*Tan et al.*, 2001]. At higher temperatures, the shear modulus becomes more strongly temperature sensitive and frequency-dependent and the dissipation increases, taking on absorption band behavior with $Q^{-1} \sim T_o^{\alpha}$ with $\alpha \sim 0.25$ for $1 < T_o < 100$ s (Figure 3). Torsional microcreep data show that such departures from the elastic ideal involve a mixture of recoverable (anelastic) and irrecoverable (viscous) strains, the proportion of the latter increasing with increasing temperature and test duration. Broad consistency between results of forced oscillation and microcreep tests along with tests at different torque amplitudes demonstrate that the stress-strain-strain rate behavior is linear in the sense defined above [*Tan et al.*, 2001].

[14] The high-temperature rheological behavior manifest in the microcreep records and in the modulus dispersion and associated strain energy dissipation can be adequately represented by a creep function $J(t)$ describing the time-dependent strain resulting from the application of Heaviside step function stress. For the alternative Andrade and extended Burgers rheologies, the creep functions are

$$J(t) = J_U + \beta t^n + t/\eta \tag{1}$$

and

$$J(t) = J_U + J_U \Delta \int_{\tau_m}^{\tau_M} [1 - e^{-t/\tau}] D(\tau) d\tau + t/\eta, \tag{2}$$

respectively. Here J_U is the unrelaxed compliance, Δ the anelastic relaxation strength, and η is the steady state viscosity. The transient term in the Andrade model takes the form βt^n with the exponent n typically between 0.2 and 0.4. For the Burgers model, a distribution $D(\tau)$ of anelastic relaxation times τ is specified as $D(\tau) \sim \tau^{\alpha-1}$ for the interval (τ_m,τ_M). The simultaneous fitting of modulus dispersion and dissipation data to such a creep function guarantees that the Kramers-Kronig relationship of linear theory is automatically satisfied [*Jackson*, 2000]. For a given specimen at a constant temperature, either of these rheological models provides an adequate description of the experimental data that includes an absorption band within which the dissipation displays an approximate power law dependence upon period with an exponent given for the Andrade and extended Burgers models by n and α, respectively [*Tan et al.*, 2001] (Figure 4).

[15] Unfortunately, such models are not readily generalized to incorporate the influence of other variables (e.g., temperature and grain size) in a parametrically economical manner. A widely used alternative description of the combined frequency and temperature dependence of strain-energy dissipation is based on the notion that Q^{-1} should

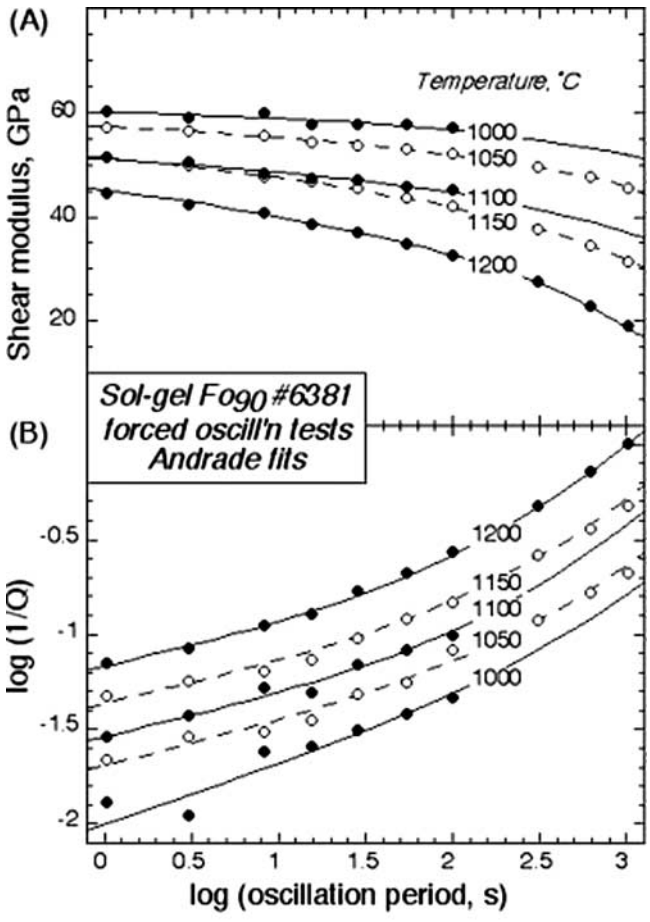

Figure 3. Representative forced oscillation data (plotting symbols) and Andrade fits (curves) to the variation of (a) shear modulus and (b) dissipation with period plotted for 50°C temperature intervals between 1000 and 1200°C.

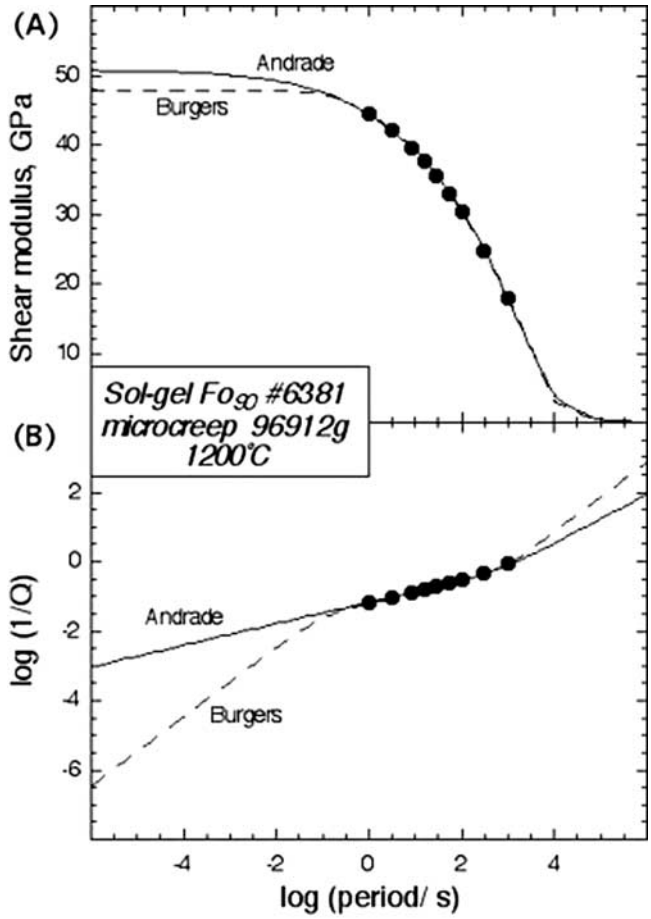

Figure 4. The period dependence of (a) shear modulus and (b) dissipation inferred from microcreep test 96912g at 1200°C on specimen 6381. The continuous and broken curves represent the alternative Andrade and Burgers models which provide equally good fits to the dispersion and dissipation within the 1-1000 s range of the observations.

be a function only of the ratio of the frequency of the mechanical test to an appropriate representative relaxation rate τ^{-1}. The temperature dependence of the latter will often be expressible through an Arrhenius relation, i.e.,

$$\tau^{-1} = v_0 \exp(-E/RT), \tag{3}$$

where v_0 is a frequency factor and E is the activation energy. Under these circumstances, Q^{-1} is a function only of the dimensionless frequency $\omega\tau$ or its reciprocal which is proportional to

$$x = T_o \exp(-E/RT). \tag{4}$$

Over restricted ranges of frequency and temperature, power law dependence of Q^{-1} upon x provides a satisfactory empirical approximation as demonstrated below. It cannot, however, be expected to apply over arbitrarily wide ranges of frequency and temperature. For example, the progressive transition at long period and high temperature to dominantly viscous behavior must lead ultimately to systematically larger values for $\partial \ln Q^{-1}/\partial \ln T_o$ given by $1-n$ or 1,

Table 3. Summary of Andrade and Burgers (B) Model Fits to Torsional Forced Oscillation and Microcreep Data (C) for Specimen 6365[a]

Run (Prior Anneal, hours)[b]	Comment	J_U, 10^{-1} GPa^{-1}	α or n	Δ or $\beta/10^{-2}$ B, GPa^{-1}s^{-n}	$\eta/10^4$ GPa s	χ^{2c}	log (τ_m/s)	log (τ_M/s)	$\tau_{Mw} = \eta J_U$, s
				Temperature 1200°C					
943-1(2)		0.181(8)	0.27(6)	0.47(8)	0.9(5)	1.09			
943-2(5)	C	0.190(5)	0.34(4)	0.48(5)	1.4(8)	0.03			270
943-3(9)		0.183(8)	0.26(6)	0.44(8)	1.2(8)	0.94			
943-4(11)	C	0.192(4)	0.34(4)	0.37(4)	2.0(13)	0.11			390
943-5(14)		0.170(8)	0.25(6)	0.42(8)	1.3(9)	1.05			
943-6(15.5)	C	0.179(4)	0.34(3)	0.42(4)	2.9(12)	0.14			520
	B	0.186(3)	0.34(4)	1.3(9)	1.7(10)	0.02	(−2)	2.7(9)	320
943-8(20)		0.173(8)	0.25(6)	0.40(8)	1.5(12)	0.73			
				Temperature 1100°C					
943-7		0.162(6)	0.21(7)	0.22(6)	3.5(29)	2.64			
943-9		0.157(5)	0.21(7)	0.23(5)	4.0(37)	1.14			
943-10	C	0.164(2)	0.38(5)	0.092(10)	5.8(44)	0.06			960
	B	0.165(2)	0.39(7)	0.22(23)	2.6(20)	0.04	(−2)	2.0(12)	430
				Temperature 1000°C					
943-11		0.150(2)	0.29(3)	0.059(7)	(10)	3.71			
				Temperature 900°C					
943-12		$\langle G\rangle$ = 66.0(6) GPa[d] $\langle Q^{-1}\rangle$ = 0.010(2)[d]							
				Temperature 800°C					
943-13		$\langle G\rangle$ = 65.6(8) GPa $\langle Q^{-1}\rangle$ = 0.010(2)							
943-14		$\langle G\rangle$ = 66.5(7) GPa $\langle Q^{-1}\rangle$ = 0.008(2)							
				Temperature 600°C					
943-15		$\langle G\rangle$ = 69.3(1) GPa $\langle Q^{-1}\rangle$ = −0.002(2)							
				Temperature 400°C					
943-16		$\langle G\rangle$ = 70.0(4) GPa $\langle Q^{-1}\rangle$ = −0.000(1)							
				Temperature 200°C					
943-17		$\langle G\rangle$ = 72.4(3) GPa $\langle Q^{-1}\rangle$ = −0.001(1)							
				Temperature 20°C					
943-18[e]		$\langle G\rangle$ = 74.2(3) GPa $\langle Q^{-1}\rangle$ = 0.002(1)							
943-19[e]		$\langle G\rangle$ = 73.0(2) GPa $\langle Q^{-1}\rangle$ = 0.001(1)							

[a]Forced oscillation data for periods of 1–100 s. Microcreep records generally of 2500 s total duration consist of (1) a 500 s interval of zero applied torque followed in turn by (2) 500 s intervals of steady (positive) torque application and recovery, and (3) as for point 2 with a negative torque of the same amplitude. The microcreep records were processed to retrieve information concerning the response at periods within the range 1–300 s. Microcreep record 943–6 of 5000 s total duration was processed to retrieve information for periods of 1–1000 s.
[b]Prior exposure to 1200°C, 200 MPa during run 943; additional 3 hour exposure during previous run 942.
[c]Based on $\sigma(G)/G$ =0.03, $\sigma(\log(1/Q))$ = 0.05.
[d]2σ in the mean for 1–100 s data.
[e]Pressure: 156 MPa for 943-18 and 98 MPa for 943-19.

respectively, for the alternative Andrade and extended Burgers rheologies [*Jackson*, 2000] (Figure 4).

5. Results

[16] The parameters of the Andrade and Burgers model creep functions that best fit the period-dependent modulus and dissipation inferred from forced oscillation and microcreep data for each of the three new specimens 6365, 6380, and 6381 at each temperature are presented in Tables 3, 4 and 5, respectively. The procedure for the calculation of $G(T\mathrm{o})$ and $Q^{-1}(T_o)$ from the parameters tabulated for the Andrade and extended Burgers models was described by *Tan et al.* [2001, Appendix].

[17] For periods T_o of 1–100 s and temperatures ranging between 1000°C and the maximum (depending upon specimen) of 1200 or 1300°C the variation of the dissipation Q^{-1} for each specimen (including 6261 from *Tan et al.* [2001]) can be adequately represented (Table 6) by a function of the form

$$Q^{-1} = Ax^{\alpha} = AT_o^{\alpha}\exp(-\alpha E/RT). \quad (5)$$

Similar behavior is observed for each of the four specimens with values for the exponent α of 0.23–0.28 and values for the activation energy E of the representative relaxation rate ranging from 397 to 495 kJ mol^{-1}. Among these specimens, those of sol-gel origin appear to display slightly higher values of α and slightly lower values of E than their counterparts derived from natural (San Carlos) olivine (Table 6).

[18] The influence of grain size is clearly demonstrated in Figure 5a by a comparison of the results of forced oscillation tests on specimens 6381, 6365, and 6261. The more fine-grained the specimen, the greater is Q^{-1} at a given temperature and oscillation period and the more strongly frequency-dependent is the shear modulus. Grain-size

Table 4. Summary of Andrade and Burgers (B) Model Fits to Torsional Forced Oscillation and Microcreep Data (C) for Specimen 6380[a]

Run (Prior Anneal, hours)[b]	Comment	J_U, 10^{-1} GPa^{-1}	α or n	Δ or $\beta/10^{-2}$ β, GPa^{-1}s^{-n}	$\eta/10^4$ GPa s	χ^{2c}	log (τ_m/s)	log (τ_M/s)	$\tau_{Mw} = \eta J_U$, s
				Temperature 1200°C					
98512a(0.5)	1–1022 s	0.190(10)	0.25(3)	0.83(11)	0.83(11)	1.6			160
98512b(12.0)	C	0.214(6)	0.33(3)	0.60(6)	1.13(29)	0.86			240
	B	0.225(4)	0.35(4)	1.18(31)	0.72(15)	0.07	(−2)	2.4(4)	160
98512c(15.0)		0.189(17)	0.23(6)	0.84(17)	0.72(43)	0.47			140
98512d(18.0)	L/2[d]	0.195(19)	0.22(6)	0.88(20)	0.63(33)	1.6			120
98512e(19.0)	C	0.212(6)	0.32(3)	0.53(5)	0.89(18)	1.6			190
	B	0.222(4)	0.35(4)	0.93(21)	0.61(9)	0.14	(−2)	2.2(3)	140
				Temperature 1150°C					
985115a	1–1022 s	0.181(7)	0.24(3)	0.54(7)	2.6(6)	2.1			470
985115b	C	0.200(4)	0.35(3)	0.34(3)	3.1(13)	0.26			630
	B	0.205(3)	0.36(4)	0.91(43)	1.7(7)	0.02	(−2)	2.5(6)	360
				Temperature 1100°C					
98511a		0.160(13)	0.18(6)	0.45(13)	3.5(39)	0.65			
98511b	C	0.180(3)	0.36(3)	0.21(2)	13(14)	0.18			
	B	0.183(2)	0.37(4)	0.72(47)	4.0(29)	0.04	(−2)	2.6(8)	740
				Temperature 1050°C					
985105a	C	0.189(2)	0.44(4)	0.059(5)	9(5)	0.95			
	B	0.190(2)	0.47(5)	0.198(74)	4.1(10)	0.28	(−2)	2.2(4)	
985105b	1–1022 s	0.177 (3)	0.26(3)	0.214(27)	14(7)	0.80			
				Temperature 1000°C					
98510a	C	0.179(2)	0.62(5)	0.016(1)	11(9)	3.9			
	B	0.180(2)	0.73(10)	0.065(22)	3.9(5)	1.4	(−2)	1.79(31)	
98510b		0.173(2)	0.37(8)	0.068(8)	12(31)	0.75			
				Temperature 900°C					
98590a		$\langle G\rangle$ = 58.0(6) GPa[e] $\langle Q^{-1}\rangle$ = 0.0144(55)[e]							
				Temperature 800°C					
98580a		$\langle G\rangle$ = 59.3(6) GPa $\langle Q^{-1}\rangle$ = 0.0081(16)							
				Temperature 700°C					
98570a		$\langle G\rangle$ = 61.8(3) GPa $\langle Q^{-1}\rangle$ = 0.0055(32)							
				Temperature 600°C					
98560a		$\langle G\rangle$ = 61.8(4) GPa $\langle Q^{-1}\rangle$ = −0.0030(16)							
				Temperature 400°C					
98540a		$\langle G\rangle$ = 62.0(1) GPa $\langle Q^{-1}\rangle$ = −0.0006(20)							
				Temperature 200°C					
98520a		$\langle G\rangle$ = 63.4(4) GPa $\langle Q^{-1}\rangle$ = 0.0011(9)							
				Temperature 20°C					
98500a[f]		$\langle G\rangle$ = 65.6(10) GPa $\langle Q^{-1}\rangle$ = 0.0056(17)							
98500b[f]		$\langle G\rangle$ = 65.9(3) GPa $\langle Q^{-1}\rangle$ = 0.0083(9)							

[a]Forced oscillation data for periods of 1–100 s unless otherwise indicated. Microcreep records of 10000 s total duration consist of (1) a 2000 s interval of zero applied torque followed in turn by (2) 2000 s intervals of steady (positive) torque application and recovery, and (3) as for point 2 with a negative torque of the same amplitude. The microcreep records were processed to retrieve information concerning the response at the same periods within the range 1–1022 s employed in the most extensive forced oscillation tests.
[b]Prior exposure to 1200°C, 200 MPa during run 985; additional 6.5 hour exposure during previous runs 983 and 984.
[c]Based on $\sigma(G)/G$ = 0.03, $\sigma(\log(1/Q))$ = 0.05.
[d]L/2 denotes halved torque amplitude.
[e]2σ in the mean for 1–100 s data (900–600°C inclusive) or 1–28 s data ($\leq$400°C).
[f]Pressure is 92 MPa for 98500a and 49 MPa for 98500b.

dependence is also evident in the general tendency for the parameter A (equation (5)) to decrease with increasing average grain size amongst the least squares fits to the data for the individual specimens (Table 6). The grain-size sensitivity of the dissipation has been quantified by inclusion in the model (equation (5)) of the additional factor d^{-m}, yielding

$$Q^{-1} = A\, d^{-m} T_o^{\alpha} \exp(-\alpha E/RT). \quad (6)$$

For the optimal fit of equation (6) to the data (N = 119) for all four specimens, A = 8.0(25) × 10^2 s$^{-\alpha}$ μm^m, m = 0.28(2), α = 0.26(1) and E = 431(24) kJ mol^{-1}. The introduction of grain-size sensitivity results in a variance reduction of 55% (Table 6). Only marginally less variance reduction (54%, Table 6) is achieved with an alternative model of the form

$$Q^{-1} = AX^{\alpha} \quad (7)$$

Table 5. Summary of Andrade and Burgers (B) Model Fits to Torsional Forced Oscillation and Microcreep Data (C) for Specimen 6381[a]

Run (Prior Anneal, hours)[b]	Comment	J_U, 10^{-1} GPa^{-1}	α or n	Δ or $\beta/10^{-2}$ β, GPa^{-1} s^{-n}	$\eta/10^4$ GPa s	χ^{2c}	log (τ_m/s)	log (τ_M/s)	$\tau_{mw} = \eta J_U$, s
				Temperature 1200°C					
96912a (0.5)		0.181(11)	0.27(6)	0.64(11)	0.38(14)	0.79			
96912c (6.0)	1-1022 s	0.184(9)	0.24(3)	0.68(10)	0.55(5)	3.6			100
96912d (18.0)		0.175(13)	0.23(6)	0.62(13)	0.43(14)	0.73			
96912e (19.5)	C, L/2[d]	0.184(7)	0.32(3)	0.73(7)	0.72(14)	2.08			130
	B	0.198(5)	0.35(4)	1.41(28)	0.47(7)	0.20	(−2)	2.2(3)	90
96912f (23.0)	L/2[d]	0.169(14)	0.22(6)	0.61(14)	0.42(13)	5.5			
96912g (25.0)		0.197(6)	0.32(3)	0.63(6)	0.71(13)	2.5			140
	B	0.209(4)	0.35(4)	1.09(21)	0.48(6)	0.27	(−2)	2.1(3)	100
96912h (28.0)		0.186(11)	0.25(6)	0.60(11)	0.54(23)	0.67			
				Temperature 1150°C					
969115a	1-1022 s	0.173(5)	0.24(3)	0.39(6)	1.6(2)	2.68			280
969115b	C	0.186(3)	0.34(3)	0.29(3)	2.0(5)	0.50			380
	B	0.191(3)	0.35(4)	0.72(26)	1.3(3)	0.12	(−2)	2.4(5)	250
				Temperature 1100°C					
96911a	C	0.189(2)	0.39(3)	0.13(1)	6.5(31)	0.51			1230
	B	0.190(2)	0.40(4)	0.40(16)	3.1(10)	0.11	(−2)	2.4(5)	600
96911b		0.180(6)	0.23(7)	0.27(6)	2.5(20)	3.1			
				Temperature 1050°C					
969105a	1-1022 s	0.166(3)	0.24(3)	0.16(3)	5.7(11)	5.2			940
969105b	C	0.175(2)	0.37(3)	0.15(2)	7.7(41)	0.23			1350
	B	0.177(2)	0.37(4)	0.50(28)	3.7(17)	0.04	(−2)	2.5(7)	650
				Temperature 1000°C					
96910b	C	0.163(2)	0.31(8)	0.070(12)	10(18)	13.4			
				Temperature 900°C					
96990a		$\langle G\rangle$ = 63.5(5)[e] GPa $\langle 1/Q\rangle$ = 0.0093(36)[e]							
				Temperature 800°C					
96980a		$\langle G\rangle$ = 63.5(6) GPa $\langle 1/Q\rangle$ = 0.0105(39)							
				Temperature 600°C					
96960a		$\langle G\rangle$ = 63.2(2) GPa $\langle 1/Q\rangle$ = −0.0007(21)							
				Temperature 400°C					
96940a		$\langle G\rangle$ = 66.1(5) GPa $\langle 1/Q\rangle$ = 0.0031(24)							
				Temperature 200°C					
96920a		$\langle G\rangle$ = 68.1(2) GPa $\langle 1/Q\rangle$ = −0.0003(9)							
				Temperature 20°C					
96900a[f]		$\langle G\rangle$ = 72.5(3) GPa[g] $\langle 1/Q\rangle$ = 0.0007(7)							
96900b[f]		$\langle G\rangle$ = 72.6(3) GPa[g] $\langle 1/Q\rangle$ = −0.0002(24)							
96900c		$\langle G\rangle$ = 71.3(3) GPa[g] $\langle 1/Q\rangle$ = 0.0009(18)							

[a]Forced oscillation data for periods of 1–100 s unless otherwise indicated. Microcreep records of 10000 s total duration consist of (1) a 2000 s interval of zero applied torque followed in turn by (2) 2000 s intervals of steady (positive) torque application and recovery, and (3) as for point 2 with a negative torque of the same amplitude. The microcreep records were processed to retrieve information concerning the response at the same periods within the range 1–1022 s employed in the most extensive forced oscillation tests.

[b]Prior exposure to 1200°C, 200 MPa during run 969; additional 3 hour exposure during previous run 968.

[c]Based on $\sigma(G)/G = 0.03$, $\sigma(\log(1/Q)) = 0.05$.

[d]L/2 denotes halved torque amplitude.

[e]2σ in the mean typically of 1–100 s data.

[f]Pressures for 96900a and 96900b are 107 and 150 MPa, respectively.

[g]Bench-top ultrasonic measurements yield V_P = 8.286(3) km s^{-1}; V_S = 4.801(2) km s^{-1} within 0.6% of the Hashin-Shtrikman average velocities calculated from single-crystal elasticity data [*Anderson and Isaak*, 1995], confirming the virtual absence of porosity.

with the controlling or "master" variable X now specified as

$$X = (T_o/d)\exp(-E/RT) \quad (8)$$

following *Kê* [1947b]. This latter model, preferred over equation (6) for reasons given in the discussion below, is compared with the dissipation data for the preferred suite of four specimens in Figure 6a where it is evident that this approach provides a "master curve" that adequately describes the variation of Q^{-1} across a wide range of conditions: $1 < T_o < 100$ s, 1000°C $< T <$ 1200–1300°C, and $2.9 \leq d \leq 23.4$ μm. The RMS deviation is about 0.1 log unit (or 20% in Q^{-1}). The moderately high value of χ^2/N (2.9) stems largely from the fact that specimen 6380 is systematically too lossy for its average (post-testing) grain

Table 6. Seismic Shear Wave Dissipation in Melt-Free Fo_{90} Olivine Polycrystals: Frequency, Temperature, and Grain-Size Sensitivity[a]

Specimen(s)[b]	Number of Data N	A[c]	α	E, kJ mol^{-1}	m	χ^2/N[d]	Variance Reduction,[e] %
6381 (sg)	35	14.1(55)	0.28(1)	441(26)	–	0.95	–
6380 (sc)	35	17.1(74)	0.25(1)	495(36)	–	1.20	–
6365 (sg)	21	4.1(13)	0.28(1)	397(22)	–	0.48	–
6261 (sc)	28	1.9(5)	0.23(1)	468(32)	–	0.81	–
All except 6380	84	1.9(9)	0.26(2)	392(35)	–	5.29	–
All except 6380[f]	84	6.0(15)	0.26(1)	420(19)	0.25(2)	1.39	74
All four	119	2.5(11)	0.26(2)	405(34)	–	6.40	–
All four[f]	119	8.0(25)	0.26(1)	431(24)	0.28(2)	2.91	55
All four[f]	119	7.5(22)	0.26(1)	424(21)	(0.26)[g]	2.93	54

[a]Dissipation data for forced oscillation periods T_o of 1–100 s and temperatures T of 1000–1200°C (except for specimen 6261 for which 1300°C data are also included) have been least squares fitted to equation (5) except as noted in footnote f.
[b]Specimens are labeled sg and sc according to their fabrication from synthetic (sol-gel) or natural (San Carlos) precursors.
[c]Unit of 10^2 s$^{-\alpha}$ for fits without grain-size sensitivity, 10^2 μm^m s$^{-\alpha}$ for fits with grain-size sensitivity.
[d]The $\chi^2/N = 1$ means that the data are fitted on average within 1σ; here 0.05 $\log_{10}$ units, equivalent to $\sigma(Q^{-1})/Q^{-1} = 0.115$.
[e]On inclusion in the model for each of the various data sets of the factor d^{-m} or $d^{-\alpha}$.
[f]Fitted by equation (6).
[g]With constraint $m = \alpha$ (i.e., equations (7) and (8)).

size (Figure 6a). A modest degree of abnormal grain growth in 6380 has resulted in a broader distribution of grain size than for the other three specimens (Figure 2), and the mechanical behavior is evidently controlled mainly by the fine-grained fraction. Although grain-size distributions have been determined for the specimens of this study (Figure 2) no attempt has yet been made to implement the suggestions of *ter Heege et al.* [2001] concerning incorporation of a measure of the breadth of the grain-size distribution into the model rheology.

[19] It is apparent from Figure 5b that the global fit (equation (8), all four specimens) provides an entirely satisfactory representation of the frequency, temperature, and grain-size sensitivity of dissipation for the specimens 6381, 6365, and 6261. Fitting of data for all specimens except 6380 results in a much improved χ^2/N (Table 6) with only a modest change in values of the fitted parameters. The favored fit to the dissipation data for the preferred absorption band data set is compared in Figure 6b with additional data for specimens 6380 and 6381 at longer periods (305, 612, and 1022 s) and with data for the more complicated Fo_{90} polycrystals of *Tan et al.* [2001] (specimens 6268 and 6328) and for the reconstituted dunite of *Gribb and Cooper* [1998]. The marked bimodality of the grain-size distribution in 6268 and dramatic grain growth in 6328 during mechanical testing precluded a quantitative estimate of grain-size sensitivity of attenuation in our previous study [*Tan et al.*, 2001]. Nevertheless, the data for these specimens, interpreted in terms of their nominal average grain sizes, are not seriously inconsistent with the newly established model (Figure 6b).

[20] Long-period data for specimens 6380 and 6381 and the data of *Gribb and Cooper* [1998] deviate systematically from the model, being higher in Q^{-1} for given X. The behavior of these most fine-grained materials ($d \leq 6.5$ μm) tested at high temperatures ($\geq$1200°C) and relatively long periods ($\geq$30 s) involves stronger frequency dependence than within the dominantly anelastic absorption band and is clearly associated with the progressive transition to viscous behavior (see discussion below). The fact that the reconstituted dunite of Gribb and Cooper must contain a significant melt fraction at temperatures above 1200°C probably explains its higher dissipation than 6380 and 6381 for given X.

[21] The grain-size sensitivity of dissipation determined from the forced oscillation tests is displayed more explicitly in Figure 7a where $\log(Q^{-1})$ is plotted against $\log(d/\mu m)$ for two representative periods (1 and 100 s) at each of two representative temperatures (1100 and 1200°C). The preferred model is indicated by the parallel lines of slope $-\alpha = -0.26$. Once again the data for specimens 6268 and 6328 of *Tan et al.* [2001] and from *Gribb and Cooper* [1998] are not grossly inconsistent with the model. Grain-size sensitivity is also evident in representative results from the microcreep tests shown in Figure 7b. Viscosities associated with Burgers model fits to these microcreep records increase systematically with increasing grain size approximately linearly with d from $4.8(6) \times 10^{12}$ Pa s for $d = 2.9$ μm (specimen 6381) to $4.6(21) \times 10^{13}$ Pa s for $d = 150$ μm (specimen 6328). The proportion of the nonelastic strain that is recoverable following removal of the applied torque decreases systematically with decreasing grain size (Figure 7b) and with increasing temperature (not shown).

[22] Of course, chemical variables such as f_{O2}, f_{H2O}, and trace impurity concentrations, along with variable dislocation density, may account for some of the variation in viscoelastic behavior observed amongst the specimens of the present study and their influence is the subject of ongoing work. However, the large reduction in variance justifies the emphasis here on grain-size-sensitivity. That the mild grain-size sensitivity (m much less than 1) is robustly inferred in spite of variable f_{H2O} is demonstrated by the results of *Tan et al.* [2001, Figure 14(c)], where 1100°C Q^{-1} data are compared for specimen 6261 and the drier and more coarse-grained specimen 6328. Attribution of the offset in Q^{-1} between these two specimens entirely to the difference in mean grain size would require $m = 0.4–0.5$. If, as is likely, the presence of trace amounts of water were to appreciably enhance dissipation, then part of the difference in Q^{-1} between specimens 6261 and 6328 should properly be associated with the difference in $[H_2O]$, implying a smaller value of m.

6. Discussion

6.1. Comparison With Previous Studies

[23] Broadly similar absorption band behavior has been described in previous studies of olivine-dominated materi-

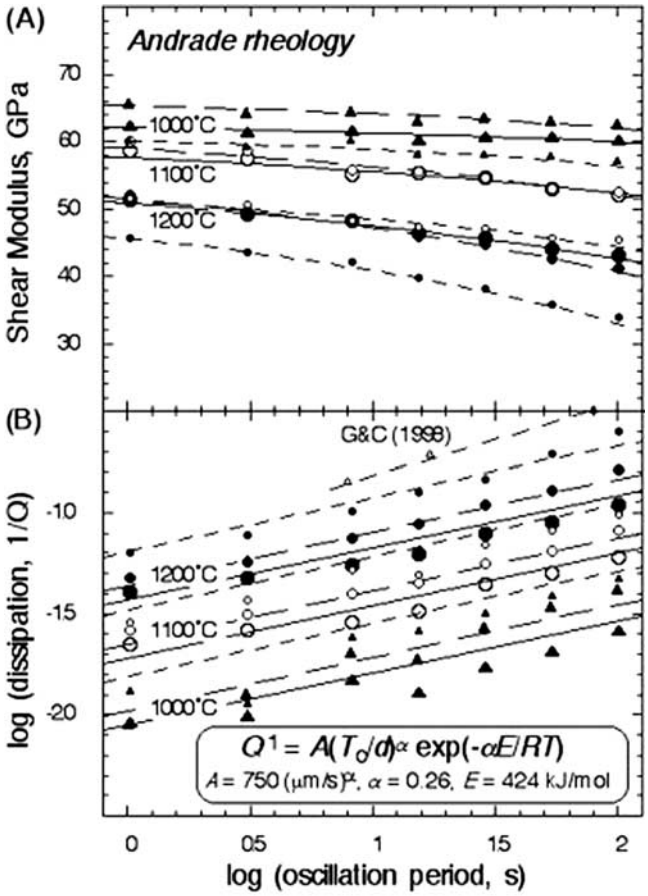

Figure 5. Grain-size sensitivity of the high-temperature mechanical behavior of olivine polycrystals. Data for specimens 6261, 6365, and 6381 of average grain size 23.4, 12.4, and 2.9 μm, are denoted by the large, medium, and small plotting symbols and by the solid, long-dashed, and short-dashed curves, respectively. Solid circles, open circles, and solid triangles denote data for 1200, 1100, and 1000°C, respectively. (a) Shear modulus. Curves labeled with temperature indicate the modulus dispersion associated with Andrade models fitted simultaneously to $G(T_o)$ and $Q^{-1}(T_o)$. (b) The log (dissipation). Lines represent the preferred fit (equations (7) and (8)) to the entire 1000–1300°C, 1-100 s data set for all four specimens, except for the uppermost line representing the results of *Gribb and Cooper* [1998] for a resynthesized dunite of 2.8 μm grain size at 1200°C.

als. Values of the power law exponent α in the frequency dependence of Q^{-1} ranging from 0.17 to 0.35 have been inferred from studies of natural olivine-rich rocks, derivative materials and synthetic forsterite single crystals [*Berckhemer et al.*, 1982; *Gueguen et al.*, 1989; *Jackson et al.*, 1992; *Tan et al.*, 1997, 2001; *Gribb and Cooper*, 1998]. Broadly comparable values for the activation energy (350–510 kJ mol^{-1}) have been reported for the dissipation measured on single-crystal forsterite [*Gueguen et al.*, 1989] and the purest of the hot-pressed olivine polycrystals [*Tan et al.*, 1997, 2001], and for steady state diffusional creep of Fo_{90} aggregates tested in conventional large-strain compressive tests [*Hirth and Kohlstedt*, 1995].

[24] The slight but potentially significant differences in power law exponent α and in activation energy between polycrystals derived from San Carlos and sol-gel precursors, mentioned in the previous section (Table 6), might be attributable to differences in their trace element inventories - especially [CaO] (Table 2). In the San Carlos-derived specimens (containing 900 wt ppm CaO) a modest degree of enrichment of grain boundary regions in Ca and Al has been reported [*Tan et al.*, 2001]. In our sol-gel derived specimens (with only 100 wt ppm CaO) neither trace amounts of melt at triple junctions nor grain boundary

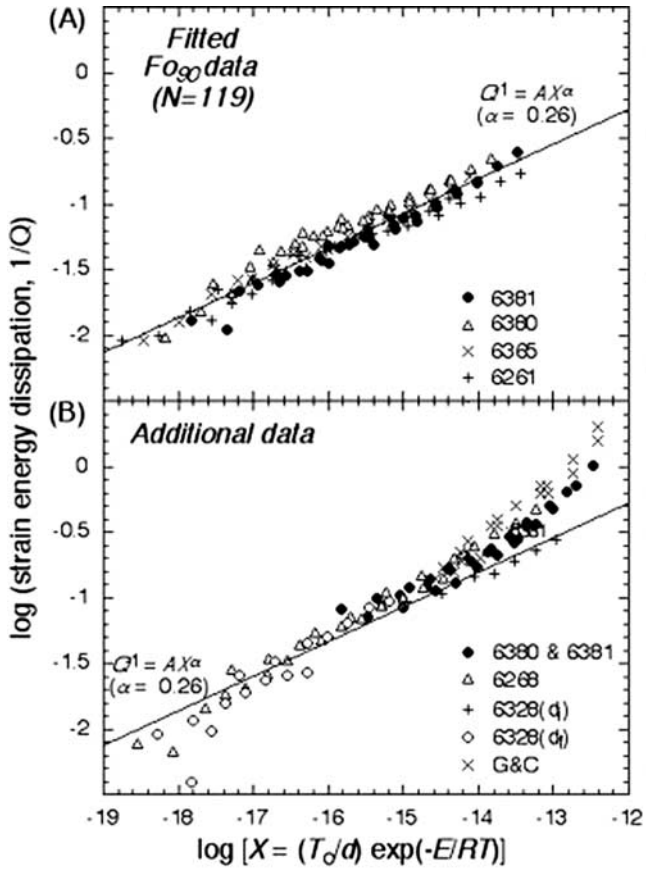

Figure 6. (a) Comparison of dissipation data with a "master curve" demonstrating the degree to which the variation of dissipation Q^{-1} with oscillation period T_o, temperature T and grain size d can be represented in terms of power law dependence upon the single variable $X = (T_o/d) \exp(-E/RT)$. The model is constrained by data for specimens 6261, 6365, 6380, and 6381 (indicated by different plotting symbols) that span the domain $1 < T_o < 100$ s, $1000 < T < 1200$°C (1300°C for specimen 6261) and $2.9 < d < 23.4$ μm. The straight line represents the preferred model with $E = 424$ kJ mol^{-1}, $\alpha = 0.26$ and $A = 750\ s^{-\alpha}\ \mu m^{\alpha}$ (Table 6). (b) Comparison of the preferred model again represented by the straight line with additional long-period (300–1000 s) data for specimens 6380 and 6381, along with data for the more complicated Fo_{90} polycrystals 6268 and 6328 of *Tan et al.* [2001] and the data for fine-grained reconstituted dunite from *Gribb and Cooper* [1998] (1200–1285°C). The labels d_i and d_f denote the average grain sizes of specimen 6328 before and after mechanical testing.

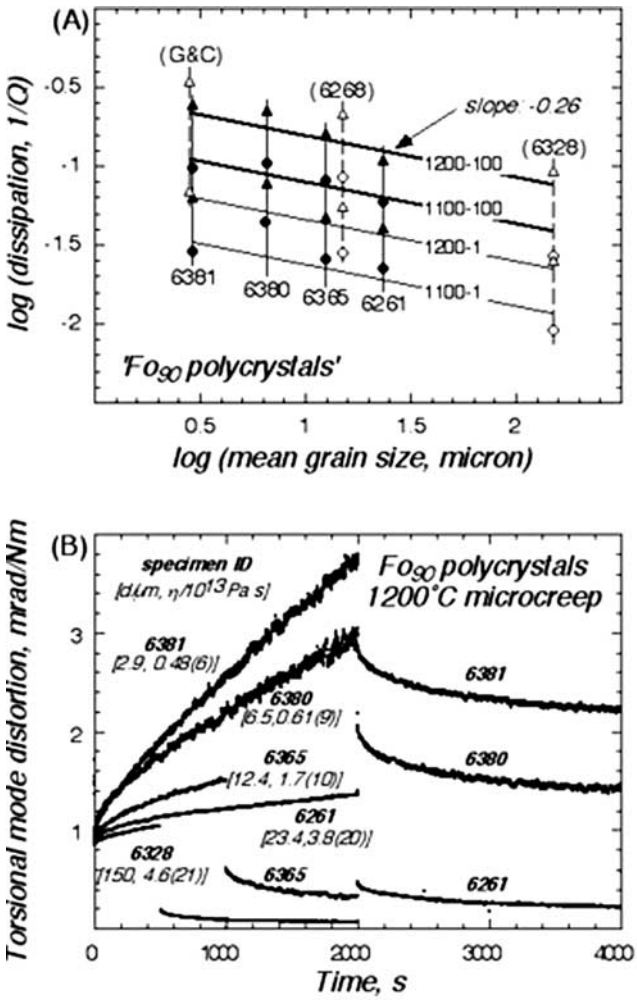

Figure 7. (a) Grain-size sensitivity of strain energy dissipation Q^{-1}. Selected data from the present study and those of *Gribb and Cooper* [1998] and *Tan et al.* [2001] are compared with the preferred model represented by the parallel lines of slope $-\alpha = -0.26$, each labeled with the relevant T (°C) $- T_o$ (s) combination. Triangles for 1200°C and circles for 1100°C; solid symbols are for specimens 6261, 6365, 6380, and 6381 used to constrain the fit, and open symbols are for other specimens. (b) Representative torsional microcreep records showing the grain-size sensitivity of the creep rate at 1200°C. Each record shows not only the creep response of the specimen assembly under constant torque but also the extent of the recovery of the nonelastic strain following the removal of the applied torque. Maximum shear strains are of the order 10^{-5}. Each curve is labeled with specimen identifier and also the mean grain size (μm) and the steady state viscosity (unit of 10^{13} Pa s) associated with the Burgers model creep function fitted to the data processed in the manner described by *Jackson* [2000].

enrichment in Ca could be detected with analytical TEM. Markedly larger values of E (640–800 kJ mol^{-1}) for dissipation have been reported for natural and reconstituted dunite [*Berckhemer et al.*, 1982; *Gribb and Cooper*, 1998], materials with much higher levels (∼ 6000 wt ppm) of CaO and other impurities.

[25] Steady state viscosities η are best constrained for the specimens of the present study by the fits of the extended Burgers rheology to the modulus dispersion and dissipation inferred from high-temperature microcreep tests (e.g., Figure 7b). For the most coarse-grained specimen (specimen 6261, $d = 23.4$ μm) at 1300°C the viscosity thus estimated is closely comparable with that calculated for the same conditions from the published flow law for grain boundary diffusional (Coble) creep in dry olivine [*Hirth and Kohlstedt*, 1995; *Drury and Fitz Gerald*, 1998]. However, the isothermal grain-size sensitivity of viscosity ($\eta \sim d^{-1}$) inferred from the microcreep tests on the various specimens of this study (Figure 7b) is much milder than that ($\eta \sim d^{-2}$ or d^{-3}) expected for Nabarro-Herring [*Bunton and Cooper*, 2001] or Coble creep, respectively. This discrepancy in the grain-size sensitivity of viscosity is not yet adequately understood.

6.2. Diffusional Mechanisms for Viscoelastic Relaxation: Models

[26] Insight into the microscopic mechanisms responsible for the nonelastic behavior observed at high temperatures and seismic frequencies in fine-grained materials requires consideration of the nature of grain boundary regions and the diffusional processes operative therein. Central to theories of grain boundary sliding is the notion of a grain boundary region, of finite width δ, distinguished from the crystalline lattices of the neighboring grains by a higher degree of positional disorder, and consequently, higher diffusivities D_{gb} for the various atomic and molecular species and lower viscosity η_{gb}. At sufficiently low temperature and/or high frequency, grain boundary sliding will be inhibited, and an unrelaxed shear modulus G_U representative of the strictly elastic behavior of the polycrystal is expected (Figure 8a). With increase of temperature and/or timescale of the mechanical test beyond an appropriate threshold, it is envisaged that the relaxation (to zero) of the distribution of grain boundary shear stress allows a finite amount of sliding along suitably oriented boundaries accommodated by elastic distortion of the neighboring grains [*Ashby*, 1972]. The modified distribution of normal stress associated with the accommodating elastic distortion provides the restoring force required for macroscopically anelastic (i.e., recoverable) behavior (Figure 8b).

[27] Analyses of simple model systems consistently yield a unique anelastic relaxation time given by

$$\tau_A = \gamma \eta_{gb} d / G_U \delta, \qquad (9)$$

linear grain size dependence

where γ, of order 1, is either a constant or a function of Poisson's ratio ν for the unrelaxed material [*Kê*, 1947a; *Nowick and Berry*, 1972; *Mosher and Raj*, 1974; *O'Connell and Budiansky*, 1977; *Ghahremani*, 1980]. The ratio of relaxed (G_R) and unrelaxed shear moduli, or alternatively the anelastic relaxation strength Δ, is also predicted by many such analyses of which the most robust and relevant is the finite element calculation of *Ghahremani* [1980] for a two-dimensional array of regular hexagons in plane strain for which

$$G_R/G_U = (1 + \Delta)^{-1} \sim 0.75 + 0.23\nu. \qquad (10)$$

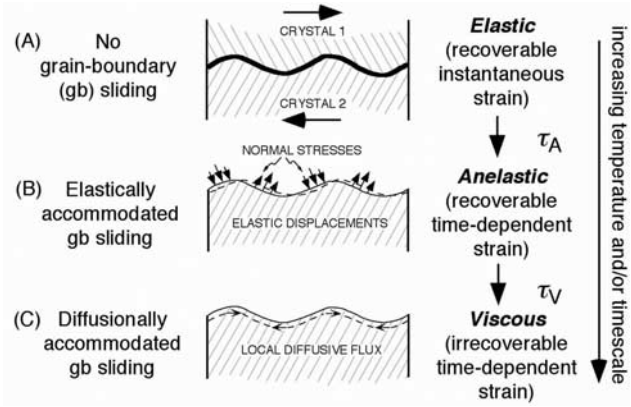

Figure 8. Grain boundary processes thought to be responsible for grain-size-sensitive seismic wave attenuation and dispersion. With increasing temperature and/or duration of the application of shear stress, a seamless transition occurs from elastic, through anelastic, to viscous behavior. The timescales for the transitions between elastic and anelastic behavior and between anelastic and viscous deformation are denoted by τ_A and τ_V, respectively. (a) Elastic deformation. Arrows indicate the sense of the imposed shear stress supported across the grain boundary. (b) Anelastic behavior. The dashed line indicates the position of the grain boundary following sliding and the accommodating elastic distortion. The arrows oriented normal to the grain boundary indicate the modified distribution of normal stress associated with the sliding and the elastic accommodation. (c) Viscous deformation in which the distribution of normal stress on the boundary is modified by local diffusive mass transfer indicated by the arrows (see text for detailed explanation; redrawn after *Ashby* [1972]).

For Fo_{90} olivine at 1000–1300°C with $\nu = 0.26$ [*Anderson and Isaak*, 1995], this analysis predicts $G_R/G_U \sim 0.81$ and $\Delta = 0.23$. In such simple model systems, both the dissipation and associated modulus reduction are expected to be strongly localized (near $X^{-1} = \omega\tau_A\ (T) = 1$) in frequency-temperature space. Such "grain boundary" dissipation peaks have been reported for various ceramic systems - often in association with an amorphous grain boundary phase of low viscosity [e.g., *Mosher et al.*, 1976; *Pezzotti et al.*, 1998].

[28] At still longer timescales and higher temperatures, it is envisaged that viscous deformation occurs with grain boundary sliding accommodated by diffusional transport of matter away from boundary regions of high chemical potential (normal stress) [*Raj and Ashby*, 1971]. The transition from the anelastic behavior associated with elastically accommodated grain boundary sliding to steady state viscous behavior requires an adjustment of the distribution of normal stress that is facilitated by grain boundary diffusion (Figure 8c). The timescale τ_V for this adjustment, which unlike τ_A is not an anelastic relaxation time, is

$$\tau_v = (1-\nu)\ kTd^3/(40\pi^3 G_U \delta D_{gb}\Omega) \qquad (11)$$

where Ω is the molecular volume of the diffusing species and k is the Boltzmann constant [*Raj*, 1975]. Now, grain boundary viscosity and diffusivity are related by

$$\eta_{gb} = f\eta^i_{gb} = fkT/8D_{gb}\Omega^{1/3}, \qquad (12)$$

where η^i_{gb} is the intrinsic viscosity of a planar boundary [*Ashby*, 1972] and f represents the enhancement of grain boundary viscosity by nanotopography and/or impurities on grain boundaries [*Crossman and Ashby*, 1975]. TEM observations on the specimens of the present study constrain grain boundary nanotopography and/or impurity particles to dimensions no more than a few nm, requiring $f < 100$. Equations (9), (11), and (12) combined yield

$$\tau_A/\tau_v = [5\pi^3 f/(1-\nu)](\Omega^{1/3}/d)^2 \sim 200f(\Omega^{1/3}/d)^2, \qquad (13)$$

implying that $3\times10^{-5}f > \tau_A/\tau_V > 3\times10^{-9}f$ for olivine with $d = 1$–100 μm at ~1200°C. Evidently, $\tau_A/\tau_V \ll 1$, meaning that theory predicts that the dissipation peak associated with the transition between elastic and anelastic behavior and the onset of appreciable distributed dissipation associated with the progressive transition between anelastic and viscous behavior should be widely separated in ω–T space.

6.3. Reconciliation of Observations and Models

[29] The results obtained in the present study depart significantly from the prescriptions of this widely used simple model of elastically and diffusionally accommodated grain boundary sliding. First, notwithstanding intensive sampling of the transition from elastic behavior through essentially anelastic into predominantly viscous deformation, dissipation peaks are conspicuous by their absence. Instead, the dissipation increases monotonically with increasing oscillation period and temperature (Figure 3b) in the manner often referred to as the high-temperature "background." For other ceramic systems lacking a widely distributed amorphous grain boundary phase, "grain boundary" Q^{-1} peaks similarly are often absent or very broad and of subsidiary significance relative to the background dissipation [*Pezzotti et al.*, 1998; *Lakki et al.*, 1999; *Webb et al.*, 1999]. Second, the microcreep tests of this study clearly demonstrate a continuous transition from elastic through anelastic to viscous behavior, implying that the timescales τ_A and τ_V are not as widely separated as suggested by the analysis given above.

[30] How are these discrepancies between simple theory and observation to be explained? Perhaps grain boundary structure and chemical composition have been seriously oversimplified in making the theory tractable? Certainly, the model grain boundaries involved in the sliding considered above are not only planar but also all of the same length (measured in the sliding direction), and of the same effective width (measured normal to the boundary) and viscosity. Variations of chemical composition or structure at the atomic scale, that might constitute impediments to grain boundary sliding, are acknowledged only through their potential to increase the effective grain boundary viscosity. However, the presence of such obstacles to sliding on entire grain boundaries might reasonably be expected to drastically broaden the dissipation peak associated with elastically accommodated grain boundary sliding or even eliminate it entirely [*Nowick and Berry*, 1972, pp. 445–446]. The full relaxation strength associated with unimpeded elastically accommodated grain

boundary sliding would then be realized progressively as increasing temperature and/or test timescale allowed local diffusional transport of matter around the obstacles to sliding. That τ_A and τ_V might not in practice be as widely separated as suggested by the above analysis is consistent with the notion whereby the relaxation of grain boundary shear stresses through local flow of grain boundary material and the relaxation of the highest-frequency Fourier components of the distribution of grain boundary normal stress involve diffusion on similarly short spatial scales.

6.4. Grain-Size Sensitivity of Q^{-1}

[31] Indications from empirical evidence and simple theoretical models concerning the frequency, temperature and grain-size sensitivity of Q^{-1} arising from the operation of diffusional processes (governed by an activation energy E) in relatively fine-grained materials are summarized in Figure 9. Where $Q^{-1} = Q^{-1}(X)$ with X prescribed by equation (8), contours of constant Q^{-1} in (ln T_o, $1/T$) space will be straight lines of slope E/R (Figure 9).

[32] Elastic behavior in the lower right-hand side of Figure 9 gives way at a threshold value of X (achieved through increasing period T_o or temperature T) to a dominantly anelastic absorption band within which the dissipation displays a mild power law dependence upon X, as in the present study where $Q^{-1} \propto X^{\alpha}$ with $\alpha \sim 1/4$. In fine-grained materials this anelastic behavior is plausibly attributed primarily to the elastically accommodated grain boundary sliding described above but with a broadly distributed rather than localized realization of the available anelastic strain as obstacles to the sliding of entire grain boundaries are progressively overcome by local diffusion around obstacles. Under these circumstances, $X \propto (\omega\tau_A)^{-1}$ is given by equation (8) thereby supporting the use of the constraint $m = \alpha$ in the preferred fit to the experimental data. A relatively small value of α ($\sim$1/4 in the present study) is thus associated with the mild frequency, temperature and grain-size sensitivity encountered within the dominantly anelastic regime close to the "elastic threshold."

[33] With increasing distance in frequency-temperature space from the lower right-hand corner of Figure 9 an increasing proportion of viscous strain signals the progressive transition from anelastic to viscous behavior. The timescale for this transition in fine-grained materials is given by equation (11) corresponding to $X \propto (\omega\tau_V)^{-1} \propto d^{-3}T_o \exp(-E/RT)$ so that here we might expect

$$Q^{-1}(T_o, T, d) \propto X^{\alpha} \propto T_o^{\alpha} d^{-3\alpha} \exp(-\alpha E/RT). \quad (14)$$

Gribb and Cooper [1998] plausibly associated their measurements at periods of 3–200 s and temperatures of 1200–1285°C on reconstituted dunite of 2.8 μm grain size with the transition between elastically accommodated and diffusionally accommodated grain boundary sliding. In this way, equation (14) reconciles the frequency dependence (α = 0.35) of Q^{-1} measured by Gribb and Cooper with the relatively strong grain-size sensitivity ($\sim d^{-1}$) required by the *Raj* [1975] model used in their extrapolation to mm grain sizes.

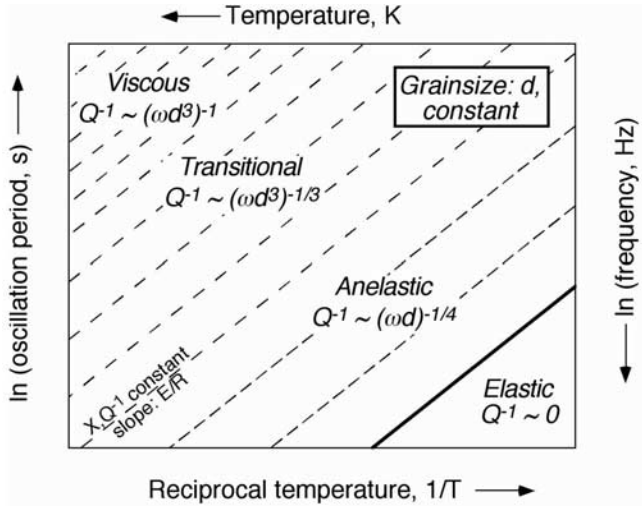

Figure 9. A schematic deformation mechanism map for the linear viscoelastic behavior encountered at very low stress and strain levels in fine-grained polycrystalline materials, illustrating the expected frequency, temperature and grain-size sensitivity of the strain energy dissipation. This map is a constant grain-size section through a three-dimensional plot in which grain size varies along the axis normal to the page. The parallel lines trending from lower left to upper right (of slope E/R) are contours of constant Q^{-1} associated with constant values of $X = (T_o/d)\exp(-E/RT)$. As X increases from its value at the elastic threshold (i.e., moving toward the upper left of the figure by increasing temperature T or period T_o) the frequency and grain-size sensitivity of the dissipation steadily strengthen. The data used to constrain the preferred model in this study ($1 < T_o < 100$ s, $1000 < T < 1200$°C (1300° only for specimen 6261) and $2.9 < d < 23.4$ μm) belong to the predominantly anelastic domain, whereas *Gribb and Cooper* [1998] plausibly ascribed their observations ($3 < T_o < 200$ s, $1200 < T < 1285$°C, $d = 2.8$ μm) on reconstituted dunite to behavior transitional between elastically accommodated grain boundary sliding (anelastic) and diffusionally accommodated grain boundary sliding (viscous), located, as indicated in this figure, further from the elastic threshold.

[34] Much further into the viscous domain, steady state Newtonian creep, represented for example by the third term in equation (2), must dominate, leading to

$$Q^{-1}(\omega, T, d) = [\omega\eta J_U(1 + \Delta)]^{-1} \propto d^{-3}T_o \exp(-E/RT), \quad (15)$$

where $\eta \sim d^3$ has been assumed for diffusionally accommodated grain boundary sliding controlled by grain boundary diffusion (i.e., Coble creep [*Frost and Ashby*, 1982]). The systematic increase from lower right to upper left in the strength of the frequency or period dependence of Q^{-1} is indicated schematically by reduced spacing between the Q^{-1} contours (Figure 9). These changes in the frequency dependence of Q^{-1} are not expected to occur abruptly at boundaries between well-defined regimes. Instead there is evidently a seamless transition from elastic through anelastic to viscous behavior with the frequency

and grain-size sensitivity both becoming progressively stronger with increasing distance from the elastic-anelastic threshold.

[35] The fact that the timescales τ_A and τ_V are each grain-size-dependent means that the threshold for the onset of appreciable anelastic behavior and the transition between elastically accommodated and diffusionally accommodated grain boundary sliding will both move (the latter further) toward the upper left of Figure 9 with increasing grain size. The result is an expansion in ($\ln T_o$, $1/T$) space of the fields for elastic and dominantly anelastic behavior for larger grain size.

6.5. Seismological Implications

[36] It follows from the foregoing analysis that extrapolation of experimental data concerning the viscoelastic behavior of fine-grained materials to the mm-cm grain sizes thought representative of the upper mantle is complicated by the systematic reduction of grain-size sensitivity as the elastic threshold is approached. Under these circumstances, the mild grain-size sensitivity ($Q^{-1} \sim d^{-1/4}$) measured in this study under conditions not far removed from the elastic threshold provides the most robust basis yet for projection of the laboratory data to upper mantle conditions.

[37] An extrapolation at 1200°C of the preferred fit from the present study to the range of grain sizes (1–10 mm) considered representative of the upper mantle is displayed in Figure 10. The influence of pressure P can be estimated by replacing the activation energy by an activation enthalpy $H = E + PV$, where V is the activation volume for the relaxation rate here assumed to be 6×10^{-6} m^3 mol^{-1} as recently estimated for climb-controlled dislocation creep [*Béjina et al.*, 1999]. The effect of 4 GPa pressure, corresponding to a representative depth of 120 km in the upper mantle, is to reduce the grain-size extrapolated Q^{-1} at 1200°C by 40% (Figure 10). The resulting ranges of dissipation at 1200°C and 4 GPa are 0.011–0.028 for 3–100 s period and 1 mm grain size and 0.006–0.015 for the same range of period at 10 mm grain size (Figure 10).

[38] It is concluded that the levels of seismic wave attenuation corresponding to the lower right-hand half of the box in Figure 10 may be attributed to grain-size-sensitive processes operative in the solid-state, notably elastically and diffusionally accommodated grain boundary sliding. Higher levels of observed seismic wave attenuation represented in the upper left-hand part of the box would require higher temperatures (as indicated by the upward arrow in Figure 10) and/or additional contributions, for example, from dislocation damping or the stress-induced redistribution of a small melt fraction. Lower levels of attenuation would require temperatures lower than 1200°C and/or average grain sizes larger than 10 mm.

[39] Furthermore, the temperature sensitivity of seismic shear wave speed is enhanced by viscoelastic relaxation. For absorption band behavior (equation (5)) the dissipation and temperature dependence of wave speed V_S are related approximately by

$$\partial \ln V_S/\partial T = \partial \ln V_{SU}/\partial T - F(\alpha)[Q^{-1}(\omega)/\pi](H/RT^2) \quad (16)$$

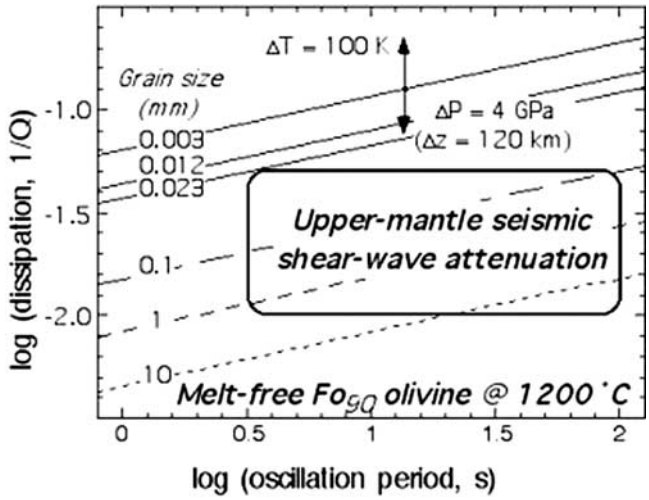

Figure 10. Extrapolation of the grain-size sensitivity of Q^{-1} measured at 1200°C to grain sizes considered representative of the upper mantle. Solid lines represent the preferred fit to experimental data obtained at 200 MPa pressure, broken lines the extrapolation at 1200°C to 0.1–10 mm grain size and the representative upper mantle pressure of 4 GPa (120 km depth). The effect of increasing temperature by 100°C is to displace these lines upwards by 0.25 log units (~1.8×), whereas a 4 GPa increase in pressure reduces the estimated dissipation by 0.22 log units (0.6×), as indicated by the arrows on the line for 0.003 mm grain size. The box represents typical observations of seismic shear wave attenuation in the upper mantle.

[*Karato*, 1993], where V_{SU} is the unrelaxed shear wave speed and $F(\alpha)$ is a function of α with a numerical value near 1. For Fo_{90} olivine at 1200°C and 4 GPa with the parameters of the present study, the term representing the viscoelastic enhancement of $\partial \ln V_S/\partial T$ assumes the value $-7.4 \times 10^{-3} Q^{-1}(\omega)$ K^{-1} to be compared with the zero-pressure value of $\partial \ln V_{SU}/\partial T = -8.6 \times 10^{-5}$ K^{-1} [*Anderson and Isaak*, 1995]. $|\partial \ln V_S/\partial T|$ is thus increased relative to the corresponding quantity for the unrelaxed wave speed by a factor varying from 1.5 at 3 s period and 10 mm grain size to 3.4 at 100 s period and 1 mm grain size.

[40] The viscoelastic enhancement of the temperature sensitivity of V_S thus results in a temperature derivative $\partial \ln V_S/\partial T$ that is strongly temperature- and frequency-dependent. The amplitudes for thermal anomalies inferred from the lateral variations in upper mantle shear wave speed should be approximately 2 to 3 times smaller than those based on unrelaxed (high-frequency) temperature derivatives. Moreover, average derivatives for finite temperature intervals will be larger at high temperature than at lower temperature [*Karato and Karki*, 2001]. It follows that tomographic wave speed anomalies arising from temperature perturbations of a given amplitude will be larger for the regions that are hotter than average than for the colder regions. Conversely, for a given magnitude of wave speed anomaly, larger temperature perturbations will be needed to

explain the negative wave speed anomalies than the positive deviations.

7. Summary

[41] Texturally mature olivine polycrystals of low porosity (<1%) have been prepared from carefully selected natural olivine phenocrysts (San Carlos) and from synthetic (sol-gel) precursor powders by hot isostatic-pressing in either Fe or $Ni_{70}Fe_{30}$ containers providing chemical environments that are more and less reducing, respectively. These Fo_{90} polycrystals with stable mean grain sizes d in the range 3–23 μm are sufficiently fine-grained to resist microcracking during thermal cycling between room temperature and peak temperatures of 1200 or 1300°C under 200 MPa confining pressure, and contain sufficiently low levels of impurity to remain demonstrably melt-free ($\ll$0.1 vol % quenched silicate melt glass) across the same temperature interval.

[42] Previously described torsional forced-oscillation techniques have been used to measure the shear modulus G and strain energy dissipation Q^{-1} on each of four such polycrystals at strain amplitudes $<10^{-5}$, for periods T_o of 1–100 s (rarely to 1000 s) and temperatures T of 20 to 1200 or 1300°C, accessed during slow staged cooling following prolonged annealing at the hot-pressing temperature. The relative magnitudes of the recoverable (anelastic) and irrecoverable (viscous) contributions to the nonelastic strain were determined in complementary torsional microcreep tests.

[43] For temperatures $\leq$900°C, the specimens behave essentially elastically with very low levels of dissipation ($Q^{-1} < 10^{-2}$) and temperature-dependent shear moduli closely consistent with expectations for a dense olivine polycrystal from MHz-frequency single-crystal elasticity data. However, increasing temperature beyond 900°C results in progressively more intense dissipation and correspondingly more pronounced frequency dependence (dispersion) of the shear modulus. For the suite of four specimens tested at temperatures of 1000 to 1200 or 1300°C and periods of 1–100 s the variation of Q^{-1} with period, temperature and grain size is adequately represented by $Q^{-1} = A\ [T_o d^{-1} \exp(-E/RT)]^{\alpha}$ with A = 7.5(22) $\times$ 10^2 $s^{-\alpha}$ μm^{α}, α = 0.26(1) and E = 424 (21) kJ mol^{-1}. For $T > 900$°C, the microcreep tests also reveal substantial departures from elastic behavior involving a mixture of anelastic and viscous contributions with the latter progressively becoming relatively more important with increasing temperature.

[44] These results along with other relevant experimental observations suggest viscoelastic behavior that is seamlessly transitional in character between elastic (for sufficiently low values of the master variable $X = (T_o/d) \exp(-E/RT)$) through anelastic (elastically accommodated grain boundary sliding) to viscous (grain boundary sliding accommodated by grain boundary diffusion).

[45] This study provides the first robust measurements of the grain-size sensitivity of strain energy dissipation in fine-grained polycrystalline olivine. These measurements intensively sampled the relatively low-loss part ($-2.0 < \log(Q^{-1}) < -0.5$, Figure 6a) of period-temperature space not far from the threshold for elastic behavior. For this reason they provide a firmer basis for extrapolation to the lower levels of dissipation expected for the larger grain sizes of the upper mantle than do the measurements of *Gribb and Cooper* [1998] that sampled a more lossy domain ($-1.0 < \log(Q^{-1}) < 0.3$, Figure 6b) further from the elastic threshold. Extrapolation (at 1200°C) of the mild grain-size sensitivity of Q^{-1} measured in this study to upper mantle grain sizes and allowance for the influence of pressure (4 GPa corresponding to a depth of 120 km), yields levels of dissipation varying with period and grain size from 0.006 at 3 s period and 10 mm grain size to 0.028 at 100 s period and 1 mm grain-size, comparable with many seismological observations.

[46] It is therefore inferred that much of the seismic wave attenuation in the upper mantle may be attributed to grain-size-sensitive diffusional processes occurring in the absence of melt, notably elastically and diffusionally accommodated grain boundary sliding. The temperature derivatives of shear wave speed associated with the levels of dissipation extrapolated to mantle grain size are enhanced 1.5- to 3.4-fold at 1200°C and 4 GPa relative to the zero-pressure unrelaxed (MHz frequency) values by the effects of viscoelastic relaxation. The enhanced temperature sensitivity of wave speeds has profound implications for the interpretation of seismic tomography: the thermal anomalies presumed responsible for the lateral velocity variations in the upper mantle must be smaller by a factor of 1.5–3.4 than would be inferred from the unrelaxed derivatives.

[47] **Acknowledgments.** The assistance of Harri Kokkonen and Joshua Carr with the preparation and characterization of the specimens for this study, Frank Brink with the EBSD, and Kay Provins and Clementine Krayshek with the preparation of the manuscript is gratefully acknowledged. Reid Cooper and Shun Karato are thanked for constructive reviews.

References

Anderson, O. L., and D. G. Isaak, Elastic constants of mantle minerals at high temperature, in *Mineral Physics and Crystallography: A Handbook of Physical Constants, AGU Ref. Shelf*, vol. 2, edited by T. J. Ahrens, pp. 64–97, AGU, Washington, D.C., 1995.

Ashby, M. F., Boundary defects and atomistic aspects of boundary sliding and diffusional creep, *Surf. Sci.*, *31*, 498–542, 1972.

Béjina, F., O. Jaoul, and R. C. Liebermann, Activation volume of Si diffusion in San Carlos olivine: Implications for upper mantle rheology, *J. Geophys. Res.*, *104*, 25,529–25,542, 1999.

Berckhemer, H., W. Kampfmann, E. Aulbach, and H. Schmeling, Shear modulus and *Q* of forsterite and dunite near partial melting from forced-oscillation experiments, *Phys. Earth Planet. Inter.*, *29*, 30–41, 1982.

Bunton, J. H., and R. F. Cooper, The impact of grain size on the shear creep and attenuation behavior of polycrystalline olivine, *Eos Trans. AGU*, *82*(47), Fall Meet. Suppl., Abstract T21C-03, 2001.

Crossman, F. W., and M. F. Ashby, The non-uniform flow of polycrystals by grain-boundary sliding accommodated by power-law creep, *Acta Metall.*, *23*, 425–440, 1975.

Drury, M. R., and J. D. Fitz Gerald, Mantle rheology: Insights from laboratory studies of deformation and phase transition, in *The Earth's Mantle: Composition, Structure and Evolution*, edited by I. Jackson, pp. 503–559, Cambridge Univ. Press, New York, 1998.

Frost, H. J., and M. F. Ashby, *Deformation-mechanism maps. The plasticity and creep of metals and ceramics*, 166 pp., Pergamon, New York, 1982.

Ghahremani, F., Effect of grain boundary sliding on inelasticity of polycrystals, *Int. J. Solids Struct.*, *16*, 825–845, 1980.

Goetze, C., A brief summary of our present day understanding of the effect of volatiles and partial melt on the mechanical properties of the upper mantle, in *High-Pressure Research: Applications in Geophysics*, edited by M. H. Manghnani and S. Akimoto, pp. 3–23, Academic, San Diego, Calif., 1977.

Grand, S. P., and D. V. Helmberger, Upper mantle shear structure beneath the Northwest Atlantic Ocean, *J. Geophys. Res.*, *89*, 11,465–11,475, 1984.

Gribb, T. T., and R. F. Cooper, Low-frequency shear attenuation in polycrystalline olivine: Grain boundary diffusion and the physical significance of the Andrade model for viscoelastic rheology, *J. Geophys. Res.*, *103*, 27,267–27,279, 1998.

Gueguen, Y., M. Darot, P. Mazot, and J. Woirgard, *Q*-1 of forsterite single crystals, *Phys. Earth Planet. Inter.*, *55*, 254–258, 1989.

Hirth, G., and D. L. Kohlstedt, Experimental constraints on the dynamics of the partially molten upper mantle: Deformation in the diffusion creep regime, *J. Geophys. Res.*, *100*, 1981–2001, 1995.

Jackson, I., Laboratory measurement of seismic wave dispersion and attenuation: Recent progress, in *Earth's Deep Interior: Mineral Physics and Tomography from the Atomic to the Global Scale, Geophys. Monogr. Ser.*, vol. 117, edited by S. Karato et al., pp. 265–289, AGU, Washington, D.C., 2000.

Jackson, I., and M. S. Paterson, A high-pressure, high-temperature apparatus for studies of seismic wave dispersion and attenuation, *Pure Appl. Geophys.*, *141*, 445–466, 1993.

Jackson, I., M. S. Paterson, and J. D. Fitz Gerald, Seismic wave attenuation in Åheim dunite: An experimental study, *Geophys. J. Int.*, *108*, 517–534, 1992.

Jackson, I., J. D. Fitz Gerald, and H. Kokkonen, High-temperature viscoelastic relaxation in iron and its implications for the shear modulus and attenuation of the Earth's inner core, *J. Geophys. Res.*, *105*, 23,605–23,634, 2000.

Karato, S., Importance of anelasticity in the interpretation of seismic tomography, *Geophys. Res. Lett.*, *20*, 1623–1626, 1993.

Karato, S., and B. Karki, Origin of lateral variation of seismic wave velocities and density in the deep mantle, *J. Geophys. Res.*, *106*, 21,771–21,783, 2001.

Kê, T., Experimental evidence of the viscous behaviour of grain boundaries in metals, *Phys. Rev.*, *71*, 533–546, 1947a.

Kê, T., Stress relaxation across grain boundaries in metals, *Phys. Rev.*, *72*, 41–46, 1947b.

Lakki, A., R. Schaller, C. Carry, and W. Benoit, High-temperature anelastic and viscoplastic deformation of fine-grained magnesia- and magnesia/yttria-doped alumina, *J. Am. Ceram. Soc.*, *82*, 2181–2187, 1999.

Mosher, D. R., and R. Raj, Use of the internal friction technique to measure rates of grain boundary sliding, *Acta Metall.*, *22*, 1469–1474, 1974.

Mosher, D. R., R. Raj, and R. Kossowsky, Measurement of viscosity of the grain-boundary phase in hot-pressed silicon nitride, *J. Mater. Sci.*, *11*, 49–53, 1976.

Nowick, A. S., and B. S. Berry, *Anelastic Relaxation in Crystalline Solids*, 677 pp., Academic, San Diego, Calif., 1972.

O'Connell, R. J., and B. Budiansky, Viscoelastic properties of fluid-saturated cracked solids, *J. Geophys. Res.*, *82*, 5719–5735, 1977.

Pezzotti, G., K. Ota, and H.-J. Kleebe, Grain-boundary viscosity of polycrystalline silicon carbides, *J. Am. Ceram. Soc.*, *81*, 3293–3299, 1998.

Raj, R., Transient behaviour of diffusion-induced creep and creep rupture, *Metall. Trans. A*, *6*, 1499–1509, 1975.

Raj, R., and M. F. Ashby, On grain boundary sliding and diffusional creep, *Metall. Trans.*, *2*, 1113–1127, 1971.

Romanowicz, B., and J. J. Durek, Seismological constraints on attenuation in the Earth: A review, in *Earth's Deep Interior. Mineral Physics and Tomography From the Atomic to the Global Scale, Geophys. Monogr. Ser.*, vol. 117, edited by S. Karato et al., pp. 161–180, AGU, Washington, D.C., 2000.

Su, W., R. L. Woodward, and A. M. Dziewonski, Degree 12 model of shear velocity heterogeneity in the mantle, *J. Geophys. Res.*, *99*, 6945–6980, 1994.

Tan, B. H., I. Jackson, and J. D. Fitz Gerald, Shear wave dispersion and attenuation in fine-grained synthetic olivine aggregates: Preliminary results, *Geophys. Res. Lett.*, *24*, 1055–1058, 1997.

Tan, B. H., I. Jackson, and J. D. Fitz Gerald, High-temperature viscoelasticity of fine-grained polycrystalline olivine, *Phys. Chem. Miner.*, *28*, 641–664, 2001.

ter Heege, J., H. de Bresser, and C. Spiers, Incorporating grain size distributions in flow laws: Implications for rheology, paper presented at Conference on Deformation Mechanisms, Rheology and Tectonics, Noorwijkerhout, Netherlands, 2001.

Toomey, D. R., W. S. D. Wilcock, S. C. Solomon, W. C. Hammond, and J. A. Orcutt, Mantle seismic structure beneath the MELT region of the East Pacific Rise and P and S wave tomography, *Science*, *280*, 1224–1227, 1998.

van der Hilst, R. D., B. L. N. Kennett, and T. Shibutani, Upper mantle structure beneath Australia from portable array deployments, *in Structure and Evolution of the Australian Continent, Geodyn. Ser.*, vol. 26, edited by J. Braun et al., pp. 39–57, AGU, Washington, D.C., 1998.

Webb, S., I. Jackson, and J. Fitz Gerald, Viscoelasticity of the titanate perovskites $CaTiO_3$ and $SrTiO_3$ at high temperature, *Phys. Earth Planet. Inter.*, *115*, 259–291, 1999.

U. H. Faul, J. D. Fitz Gerald, I. Jackson, and B. H. Tan, Research School of Earth Sciences, Australian National University, Canberra ACT 0200, Australia. (Ian.Jackson@anu.edu.au)